Breakdown of Universality in Quantum Chaotic Transport: The Two-Phase Dynamical Fluid Model

Ph. Jacquod and E.V. Sukhorukov

Département de Physique Théorique, Université de Genève, CH-1211 Genève 4, Switzerland

(Received 23 November 2003; published 16 March 2004)

We investigate the transport properties of open quantum chaotic systems in the semiclassical limit. We show how the transmission spectrum, the conductance fluctuations, and their correlations are influenced by the underlying chaotic classical dynamics, and result from the separation of the quantum phase space into a stochastic and a deterministic phase. Consequently, sample-to-sample conductance fluctuations lose their universality, while the persistence of a finite stochastic phase protects the universality of conductance fluctuations under variation of a quantum parameter.

DOI: 10.1103/PhysRevLett.92.116801 PACS numbers: 73.23.–b, 05.45.Mt, 05.45.Pq, 74.40.+k

Universal conductance fluctuations (UCF) are arguably one of the most spectacular manifestations of quantum coherence in mesoscopic systems [1]. In metallic samples, the universality of the conductance fluctuations manifests itself in their magnitude, $\mathrm{rms}(g) = O(e^2/h)$, independently on the sample's shape and size, its average conductance, or the exact configuration of the underlying impurity disorder [1,2]. In ballistic chaotic systems, a similar behavior is observed, which is captured by random matrix theory (RMT) [3]. For an open chaotic cavity connected to two N-channel leads, and thus having an average classical conductance $g = N/2$ (we consider spinless fermions and express g in units of e^2/h), RMT predicts a universal conductance variance $\sigma^2(g) = 1/8$ for time-reversal and spin rotational symmetric samples. At the core of the UCF lies the *ergodic hypothesis* that sample-to-sample fluctuations are equivalent to fluctuations induced by parametric variations (e.g., changing the energy or the magnetic field) within a given sample [1].

According to the scattering theory of transport, transport properties such as the conductance derive from transmission eigenvalues, i.e., $g = \sum_{i=1}^{N} T_i$ [4]. While coherence effects such as the UCF arise due to nontrivial correlations $\langle T_i T_j \rangle$ between pairs of different transmission eigenvalues, the knowledge of the probability distribution $P(T)$ of transmission eigenvalues is sufficient to correctly predict, e.g., the average conductance, or the Fano factor $F \equiv \langle T(1-T) \rangle / \langle T \rangle$ for the shot-noise power [5]. For a ballistic chaotic cavity, RMT predicts [3]

$$P_{\mathrm{RMT}}(T) = \frac{1}{\pi} \frac{1}{\sqrt{T(1-T)}}, \tag{1}$$

and thus $F = 1/4$. For shot noise, as for UCF, the correct universal behavior is captured by RMT.

The validity of RMT is, however, generically restricted by the existence of finite time scales. Spectral fluctuations are known to deviate from RMT predictions for energies larger than the inverse period of the shortest periodic orbit for chaotic systems [6], or than the inverse time of diffusion through the sample in disordered metallic systems [7]. Another time scale which is absent in RMT is the Ehrenfest time τ_E [8], i.e., the time it takes for the underlying classical chaotic dynamics (with Lyapunov exponent λ) to stretch an initial narrow wave packet, of spatial extension given by the Fermi wavelength λ_F, to the linear system size L. Defining $M = L/\lambda_F$, one has $\tau_E = \lambda^{-1} \ln[M/(2\tau_D)^2]$ [9,10], with $\tau_D = M/2N$, the dwell time through the cavity (all times will be measured in units of the time of flight across the cavity). Note, in particular, that the growth of τ_E in the semiclassical limit $M \to \infty$ is only logarithmic. The emergence of a finite τ_E/τ_D leads to strong deviations from the universal RMT behavior, and, in particular, to the suppression of shot noise [11–13], or the proximity gap in Andreev billiards [9,14–16]. It has furthermore been predicted that weak localization disappears at large τ_E/τ_D [17]. Also, in dirty d-wave superconductors, the RMT behavior of the quasiparticle density of states [18] is restored only below an energy scale set by τ_E [19].

The suppression of shot noise for $\tau_E/\tau_D \to \infty$ is due to the disappearance of the stochasticity of quantum mechanical transport, and its replacement by the determinism of classical transport [11–13]. Wave packets traveling on scattering trajectories shorter than τ_E have no time to diffract, and are thus either fully transmitted or fully reflected. In an open chaotic cavity, different scattering trajectories have in general different dwell times with a distribution $p(t) = \exp(-t/\tau_D)/\tau_D$. For finite $0 < \tau_E/\tau_D \ll \infty$, this suggests that transport is mediated by a two-phase dynamical fluid, consisting of a stochastic phase of relative volume $\alpha \simeq \int_{\tau_E}^{\infty} p(t)\, dt = \exp(-\tau_E/\tau_D)$, and a deterministic phase of relative volume $1-\alpha$. Following this purely classical argument, first expressed in Ref. [12], one expects that the distribution of transmission eigenvalues is given by

$$P_\alpha(T) = \alpha P_{\mathrm{RMT}}(T) + \frac{1-\alpha}{2}[\delta(T) + \delta(1-T)]. \tag{2}$$

This will be confirmed below. Building up on that we will show that, quite surprisingly, the two-phase dynamical

fluid assumption also correctly describes the behavior of mesoscopic coherent effects, and, in particular, that it explains the breakdown of universality of the conductance fluctuations when τ_E becomes comparable to the ergodic time τ_0.

We first summarize our main results. (i) We give full confirmation of Eq. (2) by calculating the integrated distribution of transmission eigenvalues $I(T) \equiv \int_0^T P(T')\,dT'$. We find that it is very well fitted by (see the inset of Fig. 1)

$$I_\alpha(T) = \frac{1-\alpha}{2}(1+\delta_{1,T}) + \frac{2\alpha}{\pi}\sin^{-1}(\sqrt{T}), \qquad (3)$$

from which we extract $\alpha \simeq \exp(-\tau_E/\tau_D)$. (ii) The conductance fluctuations stay at their universal value, independently on τ_E/τ_D, under variation of the energy in a given sample. This follows from the survival of a large number of stochastic channels — even though their relative measure $\alpha \to 0$ — which preserves the universality of the conductance fluctuations. (iii) A completely different situation arises when one considers sample-to-sample fluctuations. In this case, one has $\sigma^2(g) \propto (M/M_c)^2$ for $M > M_c$. The scaling parameter $M_c \sim \tau_D^2 \exp(\lambda)$ is determined by the quantum mechanical resolution of classical phase space structures corresponding to the largest cluster of fully transmitted or reflected neighboring trajectories (see Ref. [12]). (iv) The energy conductance correlator always decays on the universal scale of the Thouless energy, $\xi_\varepsilon \propto 1/\tau_D$, independently on τ_E. The results (ii) and (iii) show that the ergodic hypothesis breaks down as τ_E/τ_0 increases. Accordingly, (iv) is somewhat surprising, but will be understood below via a semiclassical argument. All our results and arguments fully confirm the two-phase dynamical fluid model. We note that our conclusion (iii) is in agreement with the very recent finding $\sigma^2(g) \propto M^2$ obtained by Tworzydło, Tajic, and Beenakker [20]. However, (ii) is in complete opposition with their prediction that deviations from $\sigma^2(g) = 1/8$ should occur upon variation of the energy for large τ_E/τ_D. Points (i) and (iv) are addressed here for the first time.

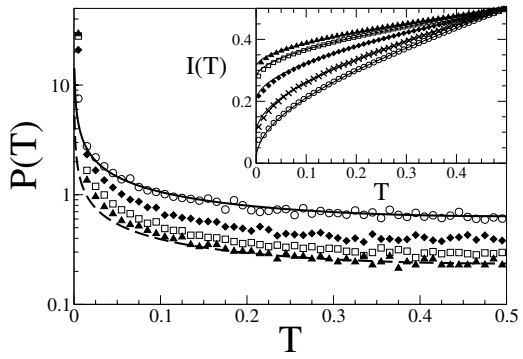

FIG. 1. Distribution of transmission eigenvalues for $K = 27.65$, $\tau_D = 25$, and $M = 2048$ (empty circles; $\tau_E \simeq 0$; distribution calculated over 729 different samples); $K = 9.65$, $\tau_D = 5$, and $M = 1024$ (black diamonds; $\tau_E = 1.5$; 729 samples); $M = 8192$ (empty squares; $\tau_E = 2.8$; 16 samples); and $M = 65536$ (black triangles; $\tau_E = 4.1$; 1 sample). The solid line gives the universal distribution P_{RMT} of Eq. (1), and the dashed line the distribution P_α of Eq. (2), with $\alpha = 0.39$. Note that $P(T)$ is symmetric around $T = 0.5$. Inset: Integrated probability distribution of transmission eigenvalues for the same set of parameters as in the main panel, as well as for $K = 9.65$, $\tau_D = 5$, and $M = 128$ ($\times$; $\tau_E = 0.16$). The solid lines are fits obtained from Eq. (3), with $\alpha \approx 0.98$, 0.81, 0.6, 0.45, and 0.385 (from bottom to top).

We consider open systems with fully developed chaotic dynamics, for which $\tau_D \gg 1$. Because τ_E grows logarithmically with M, and since we want to investigate the regime $\tau_E/\tau_D \gtrsim 1$, we model the electron dynamics by a one-dimensional map [21]. While this may seem odd at first glance, we recall that our choice of the kicked rotator map shares most of the phenomenology of low-dimensional noninteracting electronic physics [23]. The classical kicked rotator map is given by

$$\begin{cases} \bar{x} = x + p \\ \bar{p} = p + K\sin(\bar{x}), \end{cases} \qquad (4)$$

with K the (dimensionless) kicking strength. It drives the dynamics from fully integrable ($K = 0$) to fully chaotic [$K \gtrsim 7$, with Lyapunov exponent $\lambda \approx \ln(K/2)$]. We consider a toroidal classical phase space $x, p \in [0, 2\pi]$, and open the system by defining contacts to ballistic leads via two absorbing phase space strips $[x_L - \delta x, x_L + \delta x]$ and $[x_R - \delta x, x_R + \delta x]$, each of them with a width $2\delta x = \pi/\tau_D$.

Quantizing the map amounts to a discretization of, say, the real-space coordinates as $x_m = 2\pi m/M$, $m = 1, \ldots, M$. A quantum representation of the map (4) is provided by the unitary $M \times M$ Floquet operator U [22], which gives the time evolution for one iteration of the map. For our specific choice of the kicked rotator, the Floquet operator has matrix elements

$$U_{m,m'} = M^{-1/2} e^{-(iMK/4\pi)[\cos(2\pi m/M)+\cos(2\pi m'/M)]} \times \sum_l e^{2\pi i l(m-m')/M} e^{-(\pi i/2M)l^2}. \qquad (5)$$

The spectrum $\exp(i\varepsilon_\alpha)$ of U defines a discrete set of M quasienergies $\varepsilon_\alpha \in [0, 2\pi)$ with an average level spacing $\delta = 2\pi/M$.

In much the same way as the Hamiltonian case [24], a quasienergy-dependent $2N \times 2N$ scattering matrix can be determined from the Floquet operator U as [25]

$$S(\varepsilon) = P[\exp(-i\varepsilon) - U(1 - P^T P)]^{-1} U P^T, \qquad (6)$$

using a $2N \times M$ projection matrix P which describes the coupling to the leads. Its matrix elements are given by

$$P_{n,m} = \begin{cases} 1 & \text{if } n = m \in \{m_i^{(L)}\} \cup \{m_i^{(R)}\} \\ 0 & \text{otherwise.} \end{cases} \qquad (7)$$

An ensemble of samples with the same microscopic properties can be defined by varying the position $\{m_i^{(L,R)}\}$, $i = 1, \ldots, N$ of the contacts to the left and right leads for fixed $\tau_D = M/2N$ and K. We note that, from Eq. (6), S is

straightforwardly interpreted in terms of multiple scattering events between the left and right contacts.

As usual, the scattering matrix can be written in a four block form in terms of $N \times N$ transmission and reflection matrices as

$$S = \begin{pmatrix} r & t \\ t' & r' \end{pmatrix}. \tag{8}$$

The spectrum of transmission probabilities is given by the N eigenvalues T_i of $\hat{T} = tt^\dagger$, from which the dimensionless conductance is obtained, via the Landauer formula $g = \sum_i T_i$ [4]. Our numerical procedure follows the description given in Ref. [13].

We plot in Fig. 1 various distributions $P(T)$ of transmission eigenvalues. First, it is seen that our model correctly reproduces the RMT distribution of Eq. (1) in the limit $\tau_E/\tau_D \ll 1$. The distribution undergoes strong modifications, however, as τ_E/τ_D increases. In particular, more and more weight is accumulated at $T = 0$ and 1. The behavior exhibited by $P(T)$ for finite τ_E/τ_D seems very similar to that predicted by Eq. (2). To confirm this, we calculate the integrated probability distribution $I(T)$, which presents the advantage of being smoother and not dependent on the size of histogram bins, and results are shown in the inset of Fig. 1. The fitting curves clearly confirm the validity of Eq. (2). The extracted parameter α is found to obey $\alpha \approx \exp[-(1 + \tau_E)/\tau_D]$, for $\tau_E > 0$. We attribute the factor $1 + \tau_E$ in the exponential (and not τ_E) to the discrete nature of the dynamics in our model.

For $\tau_E/\tau_D \to 0$, one is in the UCF regime, where the conductance fluctuates equivalently from sample to sample or as ε is varied within a given sample. This is no longer the case, however, once τ_E becomes finite, as is shown in Fig. 2. While $\sigma^2(g) = 1/8$ seems to be preserved when ε is varied for a given sample, one gets an enormous increase $\sigma^2(g) \propto M^2$ from sample to sample. This behavior derives from the underlying classical dynamics, and can be understood on the basis of a two-phase dynamical fluid, as we now proceed to explain.

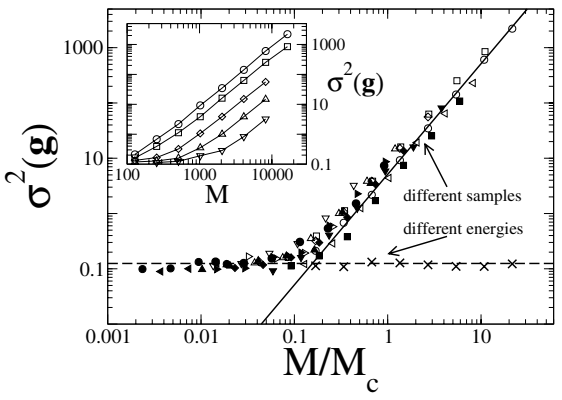

FIG. 2. Variance $\sigma^2(g)$ of the conductance vs M/M_c, for microscopic parameters $K \in [9.65, 27.65]$, $\tau_D \in [5, 25]$, and $M \in [128, 16\,384]$. The scaling parameter $M_c = 2\pi\tau_D^2 \exp(\lambda)$ varies by a factor 70. The solid and dashed lines indicate the classical, sample-to-sample behavior $\propto M^2$, and the universal behavior $\sigma^2(g) = 1/8$, respectively. Inset: Unscaled data for $K = 9.65$ and $\tau_D = 5$ (circles), 7 (squares), 10 (diamonds), 15 (upward triangles), and 25 (downward triangles).

While the classical dynamics considered here is fully chaotic, finite-sized phase space structures emerge due to the opening of the cavity, and the finiteness of $\tau_D < \infty$. Following Ref. [12], these structures can be visualized by marking which trajectories originating from, say, the left lead, end up being transmitted to the right lead, or reflected back. Such a picture is shown in Fig. 3(a). It is seen that classical trajectories are transmitted (reflected) by bands. Such bands exit the cavity at times t_j, and cover a phase space area $A_j \simeq \tau_D^{-2} \exp(-\lambda t_j)$. The shape, position, and precise volume of these bands is, of course, sample-to-sample dependent. In the semiclassical limit $\hbar_{\text{eff}} = 2\pi/M \to 0$, the effective Planck scale $\hbar_{\text{eff}}$ resolves the jth band as soon as $\hbar_{\text{eff}} \leq A_j$, or $M \geq 2\pi\tau_D^2 \exp(\lambda t_j)$. Once the largest classical band is resolved, $\sigma^2(g)$ starts to be dominated by the band fluctuations. Each resolved band carrying a growing number $\propto M$ of fully transmitted (or reflected) quantum mechanical modes; one expects a variance $\sigma^2(g) \propto (M/M_c)^2$ for sufficiently large $M > M_c$, with a scaling parameter M_c determined by the largest band, exiting the system at the ergodic time $\tau_0 \approx 1$ and, thus, $M_c = 2\pi\tau_D^2 \exp(\lambda)$. As shown in Fig. 2, this is precisely what happens [26]. Deviations from the universal behavior emerge for $M \approx M_c$, equivalently when

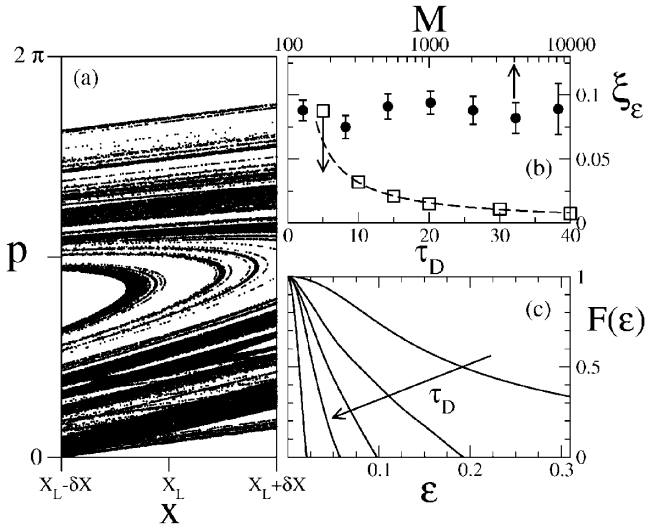

FIG. 3. (a) Phase space cross section of the left lead for $K = 9.65$, and $\tau_D = 5$. Black dots indicate transmitted, white areas reflected classical trajectories, respectively. We used 25 000 initial conditions, and only trajectories exiting the system after less than five iterations of the classical map (4) have been kept. (b) Correlation length ξ_ε extracted from the conductance correlator as $F(\xi_\varepsilon) = 0.8$, for $K = 9.65$ and $\tau_D = 5$ vs M (black circles) and for $K = 9.65$ and $M = 2048$ vs τ_D (white squares). The dashed line indicates the expected $\sim 1/\tau_D$ behavior (see text). (c) Decay of the conductance correlator $F(\varepsilon)$ vs quasienergy for $K = 9.65$, $M = 2048$, and $\tau_D = 5$, 10, 15, 20, and 40.

$\tau_E/\tau_0 \approx 1$, i.e., much earlier than the suppression of shot noise (see also Ref. [20]).

We face a completely different situation when varying ε within a given sample. In a ballistic system such as ours, such a change does not modify the classical trajectories, and thus alters only the action phase (and not the amplitude) of each contribution to the semiclassical Green function. Within this semiclassical picture, the conductance fluctuates only due to long, diffracting orbits with $t > \tau_E$ [27]. These long classical orbits build up the stochastic phase. Their subset can be viewed as corresponding to an effective stochastic cavity with contacts to leads with $N_{\text{eff}} = \alpha N$ channels. Fixing the microscopic parameters τ_D and λ, one has $N_{\text{eff}} \sim M^{1-1/\lambda\tau_D} \gg 1$. This means that, despite the prefactor α, N_{eff} is always large enough to guarantee that transport occurs semiclassically, and therefore one stays always in a regime with universal value $\sigma^2(g) = 1/8$ [3]. A first confirmation of this argument is provided by the numerical data shown in Fig. 2, which indicate a constant behavior of $\sigma^2(g)$, independently on τ_E/τ_D. To further check this argument, we finally consider the conductance correlator

$$F(\varepsilon) = \sigma^{-2}(g)\langle \delta g(\varepsilon_0)\delta g(\varepsilon_0 + \varepsilon)\rangle. \tag{9}$$

As said above, only the phase accumulated after diffraction (for $t > \tau_E$) contributes to conductance fluctuations [27] and, since the subset of diffractive trajectories have an average dwell time given by $\tau_E + \tau_D$, they accumulate a relevant relative phase $\propto \varepsilon\, \tau_D$. One therefore expects a decay of $F(\varepsilon)$ over the Thouless scale as in the universal regime [1], $\xi_\varepsilon \propto 1/\tau_D$, independently on τ_E. This is confirmed by the data shown in Figs. 3(b) and 3(c).

Our results thus show that, from the point of view of shot-noise and conductance fluctuations, the separation of the deterministic and stochastic phases is complete. Beyond a simple explanation of the suppression of shot noise with $\alpha = \exp(-\tau_E/\tau_D)$ via Eq. (2), the phase separation correctly accounts for the behavior of the conductance variance and correlators in open quantum chaotic systems in the semiclassical limit. Further investigations along the lines initiated here should focus on other effects of mesoscopic coherence, such as the weak-localization corrections and, in particular, the magnetoresistance.

We thank Marlies Goorden for a clarifying discussion of Ref. [12], and Carlo Beenakker for sending us a copy of Ref. [20]. This work was supported by the Swiss National Science Foundation.

[1] B. L. Altshuler, JETP Lett. **41**, 648 (1985); P. A. Lee and A. D. Stone, Phys. Rev. Lett. **55**, 1622 (1985).
[2] A. Benoit, C. P. Umbach, R. B. Laibowitz, and R. A. Webb, Phys. Rev. Lett. **58**, 2343 (1987); W. J. Skocpol, P. M. Mankiewich, R. E. Howard, L. D. Jackel, D. M. Tennant, and A. D. Stone, Phys. Rev. Lett. **58**, 2347 (1987).
[3] H. U. Baranger and P. A. Mello, Phys. Rev. Lett. **73**, 142 (1994); R. A. Jalabert, J.-L. Pichard, and C. W. J. Beenakker, Europhys. Lett. **27**, 255 (1994).
[4] M. Büttiker, IBM J. Res. Dev. **32**, 317 (1988).
[5] Ya. M. Blanter and M. Büttiker, Phys. Rep. **336**, 1 (2000).
[6] M. V. Berry, Proc. R. Soc. London, Ser. A **400**, 229 (1985).
[7] B. L. Altshuler and B. I. Shklovskii, Sov. Phys. JETP **64**, 127 (1986).
[8] G. P. Berman and G. M. Zaslavsky, Physica (Amsterdam) **91A**, 450 (1978); M. V. Berry and N. L. Balasz, J. Phys. A **12**, 625 (1979).
[9] M. G. Vavilov and A. I. Larkin, Phys. Rev. B **67**, 115335 (2003).
[10] The deviation from the closed sample result $\tau_E = \lambda^{-1}\ln(M)$ is due to partial reflection at the boundary between the cavity and the contacts to the leads [9].
[11] O. Agam, I. Aleiner, and A. Larkin, Phys. Rev. Lett. **85**, 3153 (2000); S. Oberholzer, E. V. Sukhorukov, and C. Schönenberger, Nature (London) **415**, 765 (2002).
[12] P. G. Silvestrov, M. C. Goorden, and C. W. J. Beenakker, Phys. Rev. B **67**, 241301 (2003).
[13] J. Tworzydło, A. Tajic, H. Schomerus, and C. W. J. Beenakker, Phys. Rev. B **68**, 115313 (2003).
[14] A. Lodder and Yu. V. Nazarov, Phys. Rev. B **58**, 5783 (1998); D. Taras-Semchuk and A. Altland, Phys. Rev. B **64**, 014512 (2001).
[15] Ph. Jacquod, H. Schomerus, and C. W. J. Beenakker, Phys. Rev. Lett. **90**, 207004 (2003); M. C. Goorden, Ph. Jacquod, and C. W. J. Beenakker, Phys. Rev. B **68**, 220501(R) (2003).
[16] A. Kormanyos, Z. Kaufmann, C. J. Lambert, and J. Cserti, cond-mat/0309306.
[17] I. L. Aleiner and A. I. Larkin, Phys. Rev. B **54**, 14 423 (1996); İ. Adagideli, Phys. Rev. B **68**, 233308 (2003).
[18] A. Altland, B. D. Simons, and M. R. Zirnbauer, Phys. Rep. **359**, 283 (2002).
[19] İ. Adagideli and Ph. Jacquod, Phys. Rev. B **69**, 020503(R) (2004).
[20] J. Tworzydło, A. Tajic, and C. W. J. Beenakker, cond-mat/0311283.
[21] Our model can be viewed as the Poincaré map defined on the boundary of the chaotic ballistic cavity [22].
[22] L. E. Reichl, *The Transition to Chaos* (Springer, New York (1992).
[23] S. Fishman, D. R. Grempel, and R. E. Prange, Phys. Rev. Lett. **49**, 509 (1984); A. Altland and M. R. Zirnbauer, Phys. Rev. Lett. **77**, 4536 (1996).
[24] S. Iida, H. A. Weidenmüller, and J. A. Zuk, Phys. Rev. Lett. **64**, 583 (1990).
[25] Y. V. Fyodorov and H.-J.Sommers, JETP Lett. **72**, 422 (2000); A. Ossipov, T. Kottos, and T. Geisel, Eurphys. Lett. **62**, 719 (2003).
[26] The estimate $A_j \simeq \tau_D^\beta \exp(-\lambda t_j)$ with $\beta = 2$, strictly applies when the beam of electrons injected into the cavity has a similar spread in momentum and real-space coordinates. For the data shown in Fig. 2, we found a significantly better numerical rescaling with $\beta \approx 1.5$ (not shown), which we relate to the anisotropy in the electron injection beam.
[27] N. Argaman, Phys. Rev. B **53**, 7035 (1996).